Kirk-Othmer Encyclopedia of Chemical Technology.

PHOTOCONDUCTIVE POLYMERS

Polymers are, in general, insulators. Some conjugated polymers, such as polyacetylene, can be made into conductors by chemical doping (see Electrically conductive polymers). Strong oxidizing agents (eg, AsF_5) and reducing agents (eg, Na) have been used as dopants (1). The function of doping can also be performed by photons if photoactive molecules are present. Certain polymers are insulators in the dark but become conductive when irradiated by light. Poly(*N*-vinylcarbazole) [25067-59-8] (PVK) was the first known photoconductive polymer (2). The discovery that PVK, when sensitized with dyes, exhibits photoconductivity high enough to be useful in electrophotography (qv) (2, 3) has stimulated extensive research in this area.

Photoconductive polymers are widely used in the imaging industry as either photosensitive receptors or carrier (electron or hole) transporting materials in copy machines and laser printers. This is still the only area in which the photoelectronic properties of polymers are exploited on a large-scale industrial basis. It is also one electronic application where polymers are superior to inorganic semiconductors.

A good photoconductive polymer should exhibit the following properties. First, it has to be a good insulator in the dark and be capable of sustaining a high electric field. The superior dielectric strength of polymers, along with their good film-forming properties, are important reasons for their success in electrophotography. Secondly, when irradiated by light, the material has to generate carriers with high quantum efficiency. The charge generation efficiencies of most polymers are low and usually have to be enhanced by doping with electron donors or acceptors. Finally, the generated carriers have to move through the polymer film without being significantly trapped. Almost all known photoconductive polymers transport holes only.

It is useful to compare the sensitivity of electrophotography with other commonly employed imaging techniques (4) (Fig. 1). The sensitivity of electrophotography is not as high as that of silver halide but is better than many other techniques, such as photopolymerization. One of the main reasons for its high sensitivity is the ability of polymer to sustain high electrical fields, which in turn enhances both the quantum yield of charge separation and the carrier mobility. In the absence of an electric field, polymers usually have low charge generation efficiency and carrier mobility.

There are many excellent reviews of photoconductive polymers (4–10). This article emphasizes results obtained after 1980, up to early 1994.

1. Classification of Materials

Photoconductive polymers can be conveniently classified into five categories based on their structures and modes of photoconduction.

1.1. Polymers With Pendent Groups

The classical photoconductive polymer, poly(*N*-vinylcarbazole) (PVK), belongs to this category. In this class of material, the polymer backbone does not participate in carrier transport directly. Instead, the carriers move

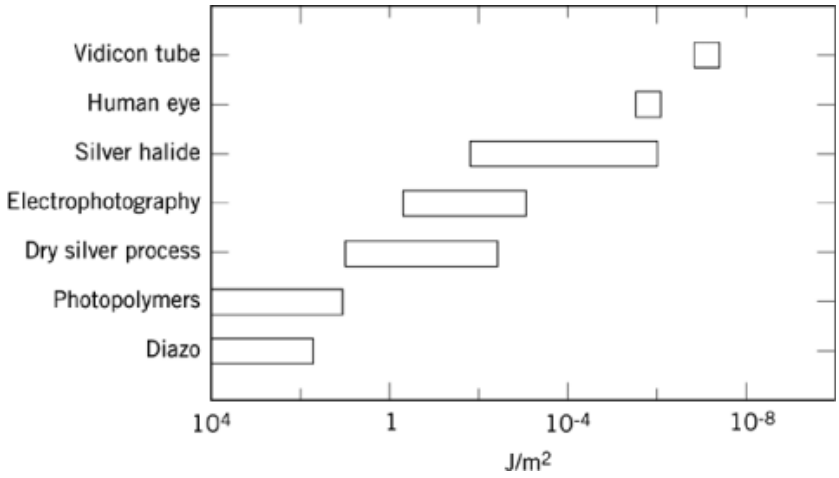

Fig. 1. Comparison of sensitivities of different imaging techniques (4).

by hopping along the electroactive pendent groups such as carbazole. These pendent groups are covalently attached to the polymers. With electron donors as the pendent group, the polymer conducts holes; with electron acceptors as the pendent group, the polymer conducts electrons. In general, only hole-conducting polymers have been successfully made with good enough properties for practical applications. The hole mobilities of this class of polymers are low, around $10^{-6} - 10^{-7}$ cm^2/Vs. Their intrinsic charge generation efficiency and spectral sensitivity range are also limited. Sensitizers such as dyes (2), 2,4,7-trinitro-9-fluorenone (11), and fullerenes (12, 13) enhance the charge generation efficiency and extend the spectral range. Most of the sensitizers are electron acceptors, which form charge-transfer complexes with the donor groups of the polymers. The excitation of the charge-transfer complexes then leads to the generation of electrons and holes. Molecular structures of selected examples of this class of polymers are shown in Figure 2.

1.2. Molecularly Doped Polymers

Many small molecules such as aromatic amines, eg, triphenylamine [603-34-9] (TPA), are excellent hole transport materials (see Table 1) (7). They can be used alone as the hole transporting layer in a device if they can be deposited as amorphous thin films. In general, however, it is more advantageous to mix them with polymers with high mechanical strength and good film-forming properties. A high concentration of hole transport molecules must be used so that the latter form an interconnecting conductive network. In this case, polymers merely act as the binders. They do not participate in carrier transport directly, but can affect the carrier mobility by modifying the trap depth and the distance between traps. The carrier mobility of this class of polymers is sensitive to the volume concentration of hole transport molecules present. Usually, the higher the concentration, the larger the hole mobility.

This class of polymeric photoconductors is distinguished from the pendent group-containing polymers, eg, PVK, by the fact that the active hole transport groups are not covalently bonded to the polymer backbone, but are merely dissolved in the polymer. This provides great flexibility for sample preparation. Different polymer matrices with different hole-transporting molecules can be combined without the need for difficult chemical synthesis. Two commonly used polymers are polycarbonate and polystyrene (Fig. 2). The molecular structures of a number of selected hole transporting molecules are shown in Figure 3.

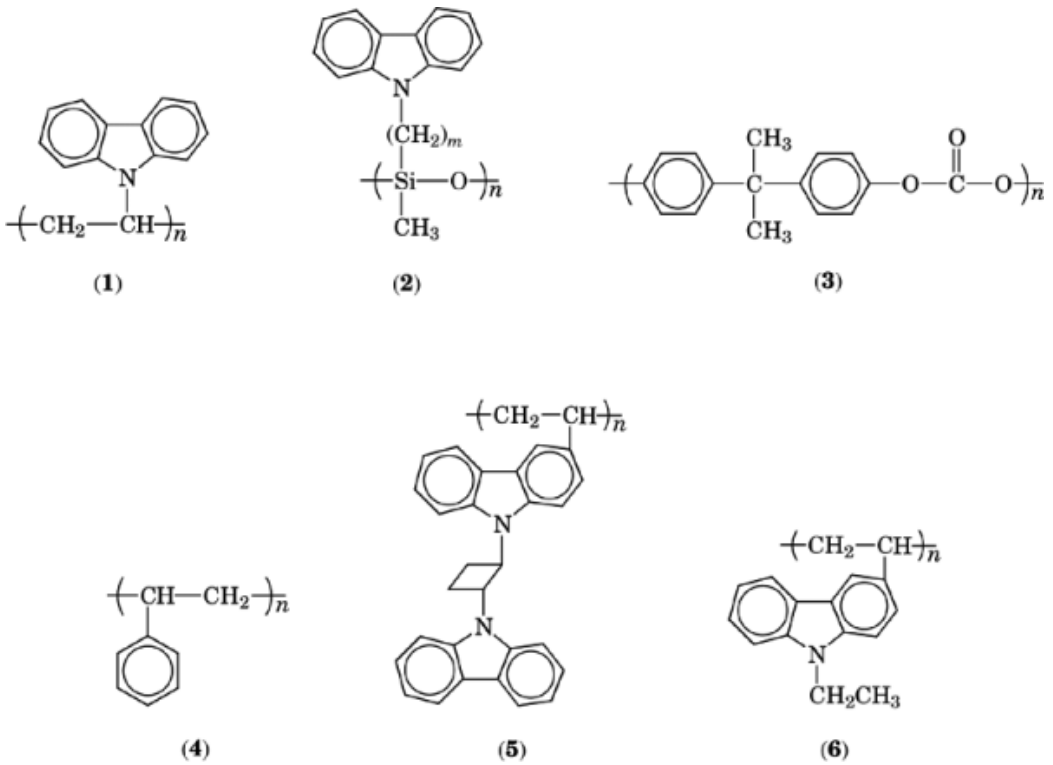

Fig. 2. Molecular structures of selected photoconductive polymers with pendent groups: (**1**) poly(*N*-vinylcarbazole) [25067-59-8] (PVK), (**2**) *N*-polysiloxane carbazole, (**3**) bisphenol A polycarbonate [24936-68-3], (**4**) polystyrene [9003-53-6], (**5**) polyvinyl(1,2-*trans*-bis(9*H*-carbazol-9-yl)cyclobutane) [80218-52-6] (PVDCZB), and (**6**) poly(9-ethyl-3-vinylcarbazole) [25569-45-3] (P3VK).

1.3. Backbone Conjugated Polymers

Polysilanes, $(RR'Si)_n$, are a unique class of polymers with the backbone consisting entirely of tetrahedrally coordinated silicon atoms. Extensive delocalization of σ-electrons takes place along the silicon chain, giving rise to many interesting electronic properties (14, 15). Because of this σ-conjugation, carrier transport along the silicon backbone is very efficient. The hole mobility of polysilanes, ca 10^{-4} cm^2/Vs (16–19) is among the highest observed for polymers. Because the hole transport is through the σ-conjugated Si backbone, the hole mobility is insensitive to the substituent on the backbone. The hole mobilities of (phenylmethyl)polysilane (PMPS), poly(*n*-dodecylmethylsilane), poly(*n*-propylmethylsilane), and poly(methylcyclohexylsilane) are essentially the same (16, 17). The charge generation efficiency and the spectral sensitivity range of polysilanes are, however, limited. Both can be enhanced by doping with sensitizers such as fullerenes (13).

Other polymers in this category include σ-conjugated polygermylenes (20) and π-conjugated polyacetylene, polythiophene, and poly(*p*-phenylenevinylene). The photoconductivity of many π-conjugated polymers can be enhanced by doping with fullerenes (21).

1.4. Liquid Crystalline Systems

Conventional photoconductive polymers are amphorous or systems with low order. In the case of PVK, the hole moves by hopping between the pendent carbazole groups. The hole mobilities are usually low, $\sim 10^{-6}$ cm^2/Vs,

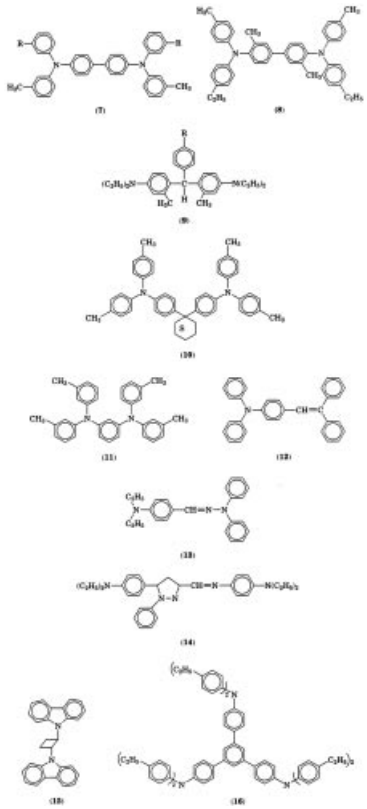

Fig. 3. Molecular structures of selected hole-transport molecules. Biphenyls: (**7a**) (R=H) *N,N′*-diphenyl-*N,N′*-bis(3-methylphenyl)-[1,1′-biphenyl]-4,4′-diamine [65181-78-4] (TPD); (**7b**) (R=CH_3) *N,N,N′,N′*-tetrakis(4-methylphenyl)-(1,1′-biphenyl)-4,4′-diamine [106614-54-4] (TTB); (**8**) *N,N′*-bis(4-methylphenyl)-*N,N′*-bis(4-ethylphenyl)-[1,1′-(3,3′-dimethyl)biphenyl]-4,4′-diamine [115310-63-9] (ETPD). Triphenylmethanes (TPM) (**9**), where R may = $-N(C_2H_5)_2$, –H, $-OCH_3$, –OH, –Br, –CN, $-NO_2$, and $-CH_3$; (**9**) (R=CH_3) is bis[4-(*N,N*-diethylamino)-2-methylphenyl](4-methylphenyl)methane [70895-80-6] (MPMP); (**10**) 1,1-bis[(di-4-tolylamino) phenyl]cyclohexane [58473-78-2] (TAPC); (**11**) tetrakis-(3-methylphenyl)-*N,N,N′,N′*-2,5-phenylenediamine [124591-08-8] (PDA); (**12**) α-phenyl-4-*N,N*-diphenylaminostyrene [89114-90-9] (TPS); (**13**) *p*-(diethylamino)benzaldehyde diphenylhydrazone [68189-23-1] (DEH); (**14**) 1-phenyl-3-[*p*-(diethylamino)styryl]5-[*p*-(diethylamino)phenyl] pyrazoline [57609-72-0] (PPR or DEASP); (**15**) 1,2-*trans*-bis(9*H*-carbazol-9-yl)cyclobutane [1484-96-4] (DCZB); and (**16**) 5′-[4-[bis(4ethylphenyl)amino]phenyl]-*N,N,N′,N′*-tetrakis(4-ethylphenyl)-1,1′:3′,1″-terphenyl-4,4″diamine (*p-p*EFTP).

due to a trap-dominated hopping transport (6–8). One approach to enhancing the hole mobility is to use conjugated polymers such as (phenylmethyl)polysilane (PMPS) (9–12). Another approach is the use of liquid crystalline systems where, in principle, transport can occur between ordered mesogenic groups (22–24).

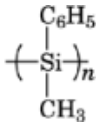

The number of examples of liquid crystalline systems is limited. A simple discotic system, hexapentyloxytriphenylene (**17**) (Fig. 4), has been studied for its hole mobility (24). These molecules show a crystalline to

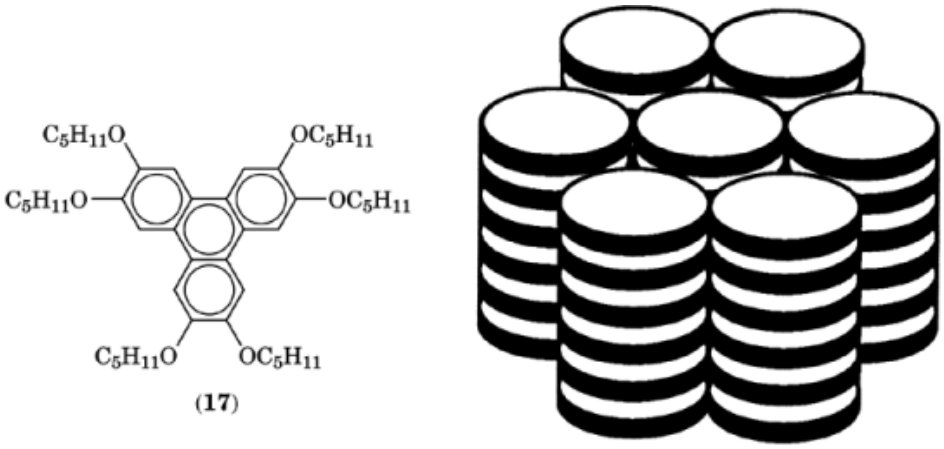

Fig. 4. Hexapentyloxytriphenylene (**17**) and a schematic view of its columnar mesophase (24).

mesophase transition at 69°C and a mesophase to isotropic phase transition at 122°C (25). In the mesophase, the molecules exist in a discotic hexagonal columnar ordered structure, schematically shown in Figure 4.

The ordered columnar arrangement of the hexapentyloxytriphenylene molecules provides good overlap of the *p*-electrons of the triphenylene moieties along the director axis. This results in efficient hole transport in the mesophase. The hole photocurrent shows nondispersive transport with a high mobility up to 1×10^{-3} cm^2/Vs (24).

1.5. Nanoclusters/Polymer Composites

The principle for developing a new class of photoconductive materials, consisting of charge-transporting polymers such as PVK doped with semiconductor nanoclusters, sometimes called nanoparticles, Q-particles, or quantum dots, has been demonstrated (26, 27).

The foundation for this new class of material is based on the ability to synthesize small semiconductor particles, typically in the nanometer-size regime (28–30). The structures of these semiconductor nanoclusters are usually the same as those of the bulk crystals, yet their properties are remarkably different. The electronic properties of these clusters depend on the cluster size, a phenomenon commonly referred to as the quantum size effect (28, 29). It is manifested as a blue-shift in the exciton energy and enhancement in the volume-normalized oscillator strength as the cluster size decreases. An exciton is an electron–hole pair bound by Coulomb interaction. With the proper surface-capping agents, clusters of varying sizes can be isolated as powders and redissolved into various organic solvents in the same manner as molecules. By co-dissolving these clusters with the polymer, a thin film of nanocluster-doped polymer can be easily made by spin-coating. Alternatively, semiconductor nanoclusters can be directly synthesized in the polymer film (26–30).

So far polymers such as PVK, polysilane, and amine-doped polycarbonate have been used as the charge-transporting matrices (26, 27). A wide variety of semiconductor nanoclusters have been synthesized within these polymers (26, 27). Many narrow gap and ir-sensitive semiconductors such as InAs normally cannot be made into high field, room temperature photoconductors for electrophotography purposes. Other than the typical difficulty of growing good quality large area thin film, the main problem is the dark decay owing to thermal excitation of carriers. By dispersing nanometer-sized InAs in charge-transporting polymers, the charge-generation efficiency of InAs is retained, but the dark decay problem is removed. An additional benefit is the ease of thin-film preparation with polymers.

This new class of photoconductive nanocluster/polymer composites have not been extensively characterized and much work remains to be done. For example, the doping of semiconductor nanoclusters was shown to enhance the charge-generation efficiency of the polymer, but the effects on the transport properties are not yet known. Inorganic semiconductors such as CdS, Si, and Se have much higher ($>10^{-1}$ cm^2/Vs) carrier mobilities than organic polymers. Many of them are also electron-transport material, unlike polymers, which are usually hole-transport material. It is therefore of interest to examine the transport properties of composites containing small inorganic clusters embedded in polymers.

2. Charge Transport

For imaging applications such as electrophotography, the speed with which the carriers (electrons or holes) move through the photoconductor is less critical than for those applications involving serial processing such as photodetectors, where nanosecond or picosecond time resolution is often required. For electrophotography, typically the carriers need to move through a ca 10-μm film in milliseconds or tens of milliseconds. This requires the polymer to have a mobility of $\geq 10^{-6}$ cm^2/Vs, which is easily achievable. More importantly, carriers have to move through the film without being trapped. It is quite remarkable that modern photoconductive polymers have been developed to the extent that polymer thin film without permanent traps can be easily fabricated. This is not the case for crystalline inorganic semiconductors, where carrier transport is extremely sensitive to the presence of impurities and fabrication of good quality thin film requires elaborate procedures.

The carrier mobility is usually measured by a time-of-flight method (31–33). The photoconductive film is sandwiched between two transparent electrodes, typically indium tin oxide and gold. The optical density of the film at the laser wavelength has to be high enough that when a low intensity, short-duration laser pulse irradiates the sample, the electron–hole pairs are created near the surface of the film. Depending on the polarity of the electric field applied on the electrodes, either electrons or holes traverse the bulk of the film. This gives rise to a displacement current that is detected by the external circuit, as shown in Figure 5**a**. In the ideal case (ie, in nondispersive transport), the current stays constant and falls off to zero at time τ_t, when the charge carriers arrive at the other side of the film. Usually the fall-off near τ_t is smeared out due to spreading of the charge carriers packet (Fig. 5**a**). The carrier mobility, μ, is then determined from the equation: $\mu = l/(\tau_t E)$, where l is the film thickness and E is the applied field.

Carrier transport in polymers is characterized by a succession of hops from site to site. The distances between various neighboring sites and the energetics of each site are different from one another. These distributions (dispersions) in energy and distance cause different hopping rates between different sites. This is called dispersive transport, which gives a transient current that deviates from the ideal shape shown in Figure 5**a**. In the extreme case, the current looks like that shown in Figure 5**b**, without any discernible break at transit time τ_t. One of the central issues in photoconductive polymer research has been to develop a theoretical framework for understanding hopping transport in polymers.

2.1. Scher-Montroll Model

In an amorphous polymer there is a distribution in the separation distances between nearest-neighbor hopping sites as well as a distribution in the energy barriers between these sites. Both distributions contribute to a strong variation in hopping times. In the case of an extremely large hopping time dispersion, the transient current displays a featureless long tail, as shown in Figure 5**b**. Such dispersive charge transport was addressed in pioneering work done during the 1970s (34, 35). It was proposed that the distribution of the hopping times, $\Psi(t)$, has the following form:

$$\Psi(t)_{t\longrightarrow\infty} \sim t^{-(1+\alpha)} \qquad 0 < \alpha < 1 \qquad (1)$$

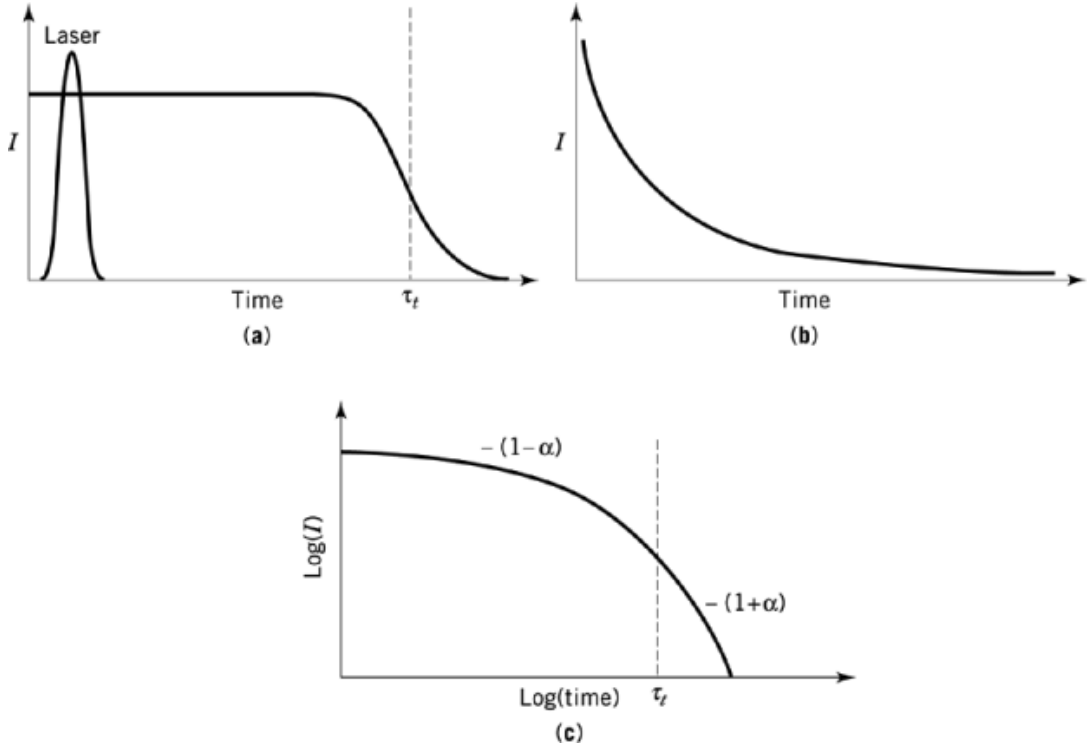

Fig. 5. Various current transients obtained by a time-of-flight method: (**a**) nondispersive transport; (**b**) dispersive transport; and (**c**) analysis of disperse current transient.

The transient current, derivable from equation 1, is given in equations 2 and 3 where τ_t is the transit time and I is the absorbed photon flux. The parameter α can be further derived as equation 4 (4), where T is the absolute temperature and T_0 is the distribution width (in units of kT) of a series of exponential traps. In this context, the carrier mobility is governed by trapping and detrapping processes at these sites.

$$I(t) \sim t^{-(1-\alpha)} \quad \text{for } t < \tau_t \qquad (2)$$

$$I(t) \sim t^{-(1+\alpha)} \quad \text{for } t > \tau_t \qquad (3)$$

$$\alpha = \frac{T}{T_0} \qquad (4)$$

According to the Scher-Montroll model, the dispersive current transient (Fig. 5**b**) can be analyzed in a double-log plot of log(I) vs log(t). The slope should be $-(1-\alpha)$ for $t < \tau_t$ and $-(1+\alpha)$ for $t > \tau_t$ with a sum of the two slopes equal to 2, as shown in Figure 5**c**. For many years the Scher-Montroll model has been the standard model to use in analyzing dispersive charge transport in polymers.

2.2. Monte Carlo Simulation

Studies using the Monte-Carlo simulation technique (7, 36, 37) have shown great success in describing the charge transport properties of polymers. In this model, charge transport occurs by hopping through a manifold of localized states with both energy and positional disorder. For energetic disorder, the energies, E, of the localized states are assumed to have a Gaussian distribution, $(2\pi\sigma^2)^{-1/2}\exp(-E^2/2\sigma^2)$, where σ is the standard deviation (distribution width). The positional disorder is due to either the fluctuation in the intersite distances or the variation of the mutual orientation, or both. The extent of the positional disorder is simulated by allowing the wavefunction overlap parameter between the two sites to fluctuate in a random manner. No analytical solution can be found for hopping transport based on this model. An analytical theory based on an effective medium approach is available (38) but it has limited applicability.

With the Monte Carlo method, the sample is taken to be a cubic lattice consisting of $70 \times 70 \times 70$ sites with intersite distance of 0.6 nm. By applying a periodic boundary condition, an effective sample size up to 8000 sites (equivalent to 4.8-μm long) can be generated in the field direction (37, 39). Carrier transport is simulated by a random walk in the test system under the action of a bias field. The simulation results successfully explain many of the experimental findings, notably the field and temperature dependence of hole mobilities (37, 39).

Figure 6 shows the field dependence of hole mobility for TAPC-doped bisphenol A polycarbonate at various temperatures (37). The mobilities decrease with increasing field at low fields. At high fields, a log $\mu \propto E^{1/2}$ relationship is observed. The experimental results can be reproduced by Monte Carlo simulation, shown by solid lines in Figure 6. The model predicts that the high field mobility follows the following equation (37) where $\hat{\sigma} = \sigma/kT$ (σ is the width of the Gaussian distribution density of states), Σ is a parameter that characterizes the degree of positional disorder, E is the electric field, μ_0 is a prefactor mobility, and C is an empirical constant given as 2.9×10^{-4} $(\mathrm{cm/V})^{1/2}$.

$$\mu(\hat{\sigma}, \Sigma, E) = \mu_0 \exp\left[-\left(\frac{2\hat{\sigma}}{3}\right)^2\right] \exp\left[C\left(\hat{\sigma}^2 - \Sigma^2\right) E^{1/2}\right] \qquad (5)$$

This equation has been used to analyze many experimental mobility data successfully, and the resultant fitting parameters are tabulated in Table 1. The value of the prefactor mobility depends on the form of the temperature dependence used. Use of a T^{-1} dependence instead of the T^{-2} dependence of equation 5 results in values that are orders-of-magnitude higher.

Based on the Monte Carlo simulations, it is seen that the presence of positional disorder causes the mobility to decrease with increasing field at low fields (37). This is the case because the introduction of positional disorder into the system provides the carrier with energetically more favorable routes, which occasionally are against the field direction. These detour routes are most efficient at low fields, but are eliminated at high fields. This rationalizes the decrease of hole mobilities with increasing field.

One potential weakness of the disorder formalism is the neglect of the polaronic effect. When an electron is transferred from the neutral form of the transport molecule to the ionic form, there is a distortion in the molecular structure, ie, the formation of a polaron, in physicists' language. The polaron model considers this intramolecular deformation energy to be more important than the disorder energy (40–43). In general, such deformation must occur during charge transport and should be considered in the next level of the disorder formalism. Guidelines for estimating the polaronic effect have been discussed and it is believed that this effect usually is small (7).

2.3. Experimental Hole Mobilities

The experimental values of hole mobilities in polymers are tabulated in Tables 1 and 2. The hole mobility is field dependent. Whenever the experimental data have been fitted with equation 5, the parameters μ_0, σ, and

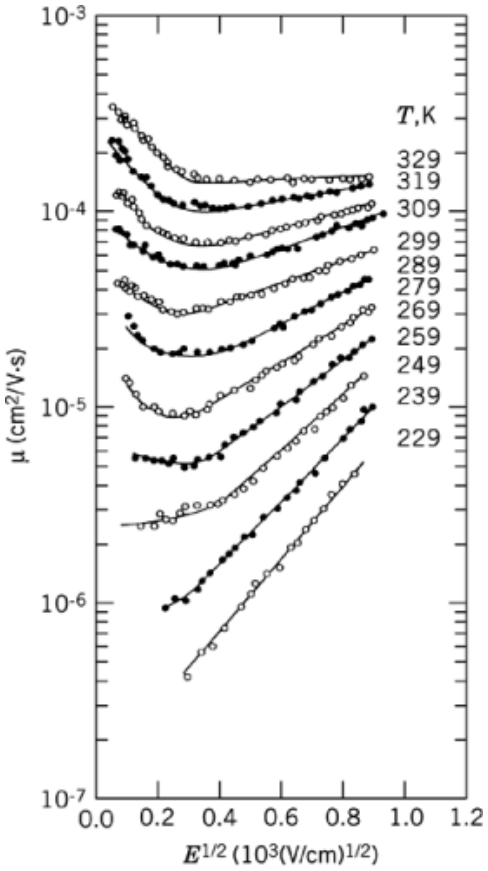

Fig. 6. The logarithm of the mobility vs $E^{1/2}$, parametric in temperature, for TAPC-doped polycarbonate (37).

σ, which give a complete description of the field dependence of the hole mobility, are listed (Table 2). Otherwise, hole mobilities at selected fields are listed. All acronyms are defined in Figures 2 and 3.

The values of the hole mobilities for polymers span a large range, from ca 10^{-10} cm^2/Vs to ca 10^{-1} cm^2/Vs. Polymers with pendent groups such as PVK tend to have the smallest mobilities (Table 1, entries 1 to 13). The mobility depends on the average separation distance between the pendent groups (Table 1, entries 6–8) (47). Polymers with conjugated backbones (Table 1, entries 14–23) and molecularly doped polymers (Table 1, entries 24–50 and all Table 2 entries) generally have higher mobilities. As a class, the transport properties of molecularly doped polymers have been studied more systematically because of the flexibility in sample fabrication. Several interesting effects and trends have been observed.

Table 1. Hole Mobilities of Selected Molecular and Polymeric Materials[a]

Entry	Materials	Hole mobility, $cm^2/V{\cdot}s$	Reference
1	PVK	10^{-6} at 5×10^5 V/cm; 10^{-7} at 5×10^4 V/cm	44
2	10% TNF/PVK	3×10^{-6} at 1×10^6 V/cm; 10^{-7} at 1×10^5 V/cm	11
3	1% C-60/PVK	2×10^{-7} at 3×10^5 V/cm; 10^{-6} at 7×10^5 V/cm	45
4	P3VK	1.9×10^{-7} at 4×10^5 V/cm	46
5	PVDCZB	3.2×10^{-6} at 4×10^5 V/cm	46
6	*N*-polysiloxanecarbazole, $m = 3$	ca 10^{-7} at 2.5×10^5 V/cm and 263 K	47

Table 1. ***Continued***

Entry	Materials	Hole mobility, $cm^2/V{\cdot}s$	Reference
7	*N*-polysiloxanecarbazole, $m = 5$	ca 2×10^{-8} at 2.5×10^5 V/cm and 263 K	47
8	*N*-polysiloxanecarbazole, $m = 6$	ca 10^{-8} at 2.5×10^5 V/cm and 263 K	47
9	0.01% TPD/PVK	ca 3×10^{-7} at 3×10^5 V/cm	(48, 49)
10	1% TPD/PVK	ca 3×10^{-9} at 3×10^5 V/cm	(48, 49)
11	60% TPD/PVK	ca 10^{-4} at 3×10^5 V/cm	(48, 49)
12	PTPB	10^{-5} at 3×10^5 V/cm	50
13	poly(hydroxyamino ester) (PHA)	2×10^{-6} at 8×10^5 V/cm	51
14	(phenylmethyl)polysilane (PMPS)	10^{-4} at 2×10^5 V/cm; 3×10^{-4} at 1×10^6 V/cm	(16, 17)
15	1%C-70/PMPS	9×10^{-5} at 3×10^4 V/cm; 1.4×10^{-3} at 4×10^5 V/cm	45
16	1% TPD/PMPS	ca 10^{-4} at 3×10^5 V/cm	48
17	1% DEH/PMPS	ca 10^{-6} at 3×10^5 V/cm	48
18	1% PPR/PMPS	ca 5×10^{-8} at 3×10^5 V/cm	48
19	50% TPS/PMPS	10^{-3} at 2×10^5 V/cm	52
20	50% PDA/PMPS	10^{-3} at 2×10^5 V/cm	52
21	60% TPD/PMPS	8×10^{-4} at 2.5×10^5 V/cm	48
22	75% ETPD/PMPS	ca 10^{-1} at 2.5×10^5 V/cm	48
23	PDBG	ca 10^{-4}	(20, 53)
24	10% TPD/polystyrene	ca 10^{-8} at 10^5 V/cm	54
25	20% TPD/polystyrene	ca 10^{-6} at 10^5 V/cm	54
26	50% TPD/polystyrene	ca 10^{-4} at 10^5 V/cm	54
27	75% TPD/polystyrene	ca 2×10^{-4} at 10^5 V/cm	54
28	10% TPD/polycarbonate	ca 10^{-10} at 10^5 V/cm	54
29	75% TPD/polycarbonate	ca 5×10^{-5} at 10^5 V/cm	54
30	10% ETPD/polystyrene	ca 10^{-7} at 10^5 V/cm	54
31	20% ETPD/polystyrene	ca 10^{-5} at 10^5 V/cm	54
32	50% ETPD/polystyrene	ca 5×10^{-4} at 10^5 V/cm	54
33	75% ETPD/polystyrene	ca 10^{-3} at 10^5 V/cm	54
34	10% ETPD/polycarbonate	ca 10^{-8} at 10^5 V/cm	54
35	75% ETPD/polycarbonate	ca 10^{-4} at 10^5 V/cm	54
36	70% DEASP/polystyrene	6×10^{-7} at 4×10^4 V/cm; 2×10^{-5} at 6×10^5 V/cm	43
37	10% DEASP/polystyrene	4×10^{-9} at 1×10^6 V/cm	43
38	70% DEASP/polycarbonate	6×10^{-7} at 4×10^4 V/cm; 2×10^{-5} at 6×10^5 V/cm	43
39	10% DEASP/polycarbonate	1.3×10^{-9} at 1×10^6 V/cm	43
40	50% DEH/polycarbonate	ca 1×10^{-7} at 6×10^4 V/cm; ca 1×10^{-6} at 1×10^6 V/cm	55
41	20% TPA/polycarbonate	10^{-6} at 5×10^5 V/cm	(56, 57)
42	45% TPA/polycarbonate	10^{-5} at 5×10^5 V/cm	(56, 57)
43	TPM, R = $-N(C_2H_5)_2$	8×10^{-4} at 5×10^5 V/cm	58
44	TPM, R = –H	1×10^{-5} at 5×10^5 V/cm	58
45	TPM, R = $-OCH_3$	3×10^{-6} at 5×10^5 V/cm	58
46	TPM, R = –OH	7×10^{-7} at 5×10^5 V/cm	58
47	TPM, R = –Br	7×10^{-7} at 5×10^5 V/cm	58
48	TPM, R = –CN	5×10^{-8} at 5×10^5 V/cm	58
49	TPM, R = $-NO_2$	2×10^{-8} at 5×10^5 V/cm	58
50	thiapyrylium dye aggregates in TPM/polycarbonate	ca 10^{-8} at ca 10^5 V/cm	59
51	discotic mesophase of hexa-pentyloxytriphenylene (HPT)	10^{-3} from 1×10^4 to 3×10^5 V/cm	24
52	DCZP/poly(11-(4-cyano-4′-biphenyl)-1-undecanoyl acrylate	10^{-6} at 6×10^5 V/cm	60

[a]All acronyms are defined in Figures 2 and 3.

Table 2. μ_0,σ, and Σ and Some Hole Mobilities, cm^2 / V·s, of Selected Molecular and Polymeric Materials[a]

Entry	Materials	μ_0, cm^2/V·s	σ, eV	Σ	Ref.
1	1,1-bis[(di-4-tolylamino) phenyl] cyclohexane (TAPC)	0.13	0.068	1.0	61
2	75% TAPC/polystyrene[b]	0.23	0.077	2.14	62
3	75% TAPC/polycarbonate[c]	0.02	0.095	3.1	62
4	40% TAPC/styrene:butylacrylate copolymers, S:BA = 100:0	1.5×10^{-2}	0.069	2.4	63
5	40% TAPC/styrene:butylacrylate copolymers, S:BA = 95:5	1.7×10^{-2}	0.073	2.4	63
6	40% TAPC/styrene:butylacrylate copolymers, S:BA = 85:15	1.7×10^{-2}	0.08	2.4	63
7	40% TAPC/styrene:butylacrylate copolymers, S:BA = 75:25	1.6×10^{-2}	0.086	2.4	63
8	40% TAPC/styrene:butylacrylate copolymers, S:BA = 50:50	1.5×10^{-2}	0.103	2.4	63
9	40% TAPC/poly(4-*tert*-butylstyrene)	1.5×10^{-2}	0.077	2.4	64
10	40% TAPC/poly(4-chlorostyrene)	1.3×10^{-2}	0.087	2.4	64
11	*N,N′*-diphenyl-*N,N′*-bis(3-methyl-phenyl)-[1,1′-biphenyl]-4,4′-diamine (TPD)[d]	0.035	0.074	1.2	(61, 65)
12	1-phenyl-3-[*p*-(diethylamino)styryl]-5-[*p*-(diethylamino)phenyl] pyrazoline (DEASP or PPR)	0.006	0.103	1.4	61
13	*p*-(diethylamino)benz-aldehyde diphenylhy-drazone (DEH)	0.0013	0.1	2.0	61
14	*N,N,N′,N′*-tetrakis(4-methyl-phenyl) (1,1′-biphenyl)-4,4′-diamine (TTB)	0.019	0.069	1.5	61
15	bis[4-(N,N-diethylamino)-2-methyl-phenyl](4-methylphenyl)-methane (MPMP) 5′-[4-[bis(4-ethylphenyl)amino]-phenyl]-*N,N,N′,N′*-tetrakis(4-ethylphenyl)-1,1′:3′,1″-terphenyl-4,4″-diamine	0.34	0.098	2.0	61
16	(*p*-*p*EFTP)	0.069	0.068	1.0	66

[a]The hole mobility is field-dependent and only selected low field and high field values are listed here. All data were measured at room temperature unless otherwise noted. All acronyms are defined in Figures 2 and 3.
[b]Hole mobilities, cm^2/V·s, = 6×10^{-3} at 4×10^4 V/cm; 1×10^{-2} at 5×10^5 V/cm.
[c]Hole mobilities, cm^2/V·s, = 4×10^{-5} at 4×10^4 V/cm; 6×10^{-5} at 5×10^5 V/cm.
[d]Hole mobility = ca 10^{-3} at 10^5 V/cm.

In molecularly doped polymers, charge transport is carried out by the hole-transporting molecular dopants, usually aromatic amines. The polymer merely acts as a binder. The hole mobility is sensitive to the dopant concentrations. For example, the hole mobility of *N,N′*-diphenyl-*N,N′*-bis(3-methylphenyl)-[1,1′-biphenyl]-4,4′-diamine [65181-78-4] (TPD) (3**a**) in polystyrene is ca 10^{-8} cm^2/Vs at 10^5 V/cm with 10% TPD concentration but increases to ca 2×10^{-4} cm^2/Vs with 75% TPD concentration (entries 24–27 of Table 1) (54).

Although polymers do not participate in carrier transport directly, they can affect the carrier mobility by modifying the carrier trap depth and distribution. For example, the hole mobility of 1,1-bis[(di-4-tolylamino) phenyl]cyclohexane [58473-78-2] (TAPC) 3 doped polystyrene is about 100 times larger than that of TAPC-doped polycarbonate (Table 2, entries 2 and 3) (37). The σ-parameter, which measures the energetic disorder, decreases when polycarbonate is replaced by polystyrene. This change is attributed to the elimination of dipolar fields generated by the carbonyl groups of the polycarbonate (62). It was also observed that the μ_0 parameter increases by an order of magnitude in conjunction with a decrease in σ from polycarbonate to polystyrene (Table 2). This suggests that intermolecular electronic coupling between TAPC molecules is improved by the reduction of positional disorder in polystyrene (62). The same effect was also observed when copolymers of styrene and butyl acrylate were used as the matrices (63). It was found that the higher the styrene content, the smaller the σ-value and the higher the mobility (Table 2, entries 4–8). This is attributed to the increase of energetic disorder owing to the polar carbonyl groups in butyl acrylate (63). Studies using other hole-transporting molecules such as TPD and ETPD show the same striking effects on the hole mobility by the host polymers (Table 1, entries 24–35) (54).

The effects of the dipole moment on the hole mobility are clearly illustrated in a study using a series of hole-transporting amines with different dipole moments (61). The mobility data can be analyzed using equation 5. It was found that amines with a large dipole moment have large σ and lower mobility (Table 2, entries 1 and 11–14) (61). This again confirms the detrimental effects of polar groups on the carrier mobility in amorphous systems.

Interesting effects are observed when "transport-active" polymers are treated with various dopants. At low dopant concentrations, the hole mobility is expected to be the same as that of the host polymer with minimum perturbation from the dopant (eg, Table 1, entries 3, 9, and 15). However, even at low dopant concentrations, decreases in hole mobility have been observed when the oxidation potential of the dopant is much lower than that of the host. For example, the hole mobility of (phenylmethyl)polysilane [76188-55-1] (PMPS) scales qualitatively with the oxidation potential of the dopants TPD, *p*-(diethylamino)benzaldehyde diphenylhydrazone [68189-23-1] (DEH) 3, and 1-phenyl-3-[*p*-(diethylamino)styryl]-5-[*p*-(diethylamino)phenyl] pyrazoline [57609-72-0] (PPR) 3 (all 1% doping) (48). A hole mobility of 10^{-4} cm^2/Vs exists for TPD-doped PMPS, while PPR-doped PMPS has a mobility of only 5×10^{-8} cm^2/Vs (Table 1, entries 16–18). The dopant PPR, having a low oxidation potential, acts as a deep trap and reduces the hole mobility.

At very high dopant concentrations, transport occurs directly between the dopant molecules. The polymer acts only as a binder in most cases. Taking TPD-doped PVK as an example, at low TPD concentrations the hole mobility first decreases from 3×10^{-7} cm^2/Vs to 10^{-9} cm^2/Vs with increasing TPD concentration, because TPD molecules act as hole traps (48, 49). At higher TPD concentrations, new direct transport channels between the TPD molecules open up and the hole mobility increases to 10^{-4} cm^2/Vs for ca 60% TPD doping (Table 1, entries 9–11) (48, 49). In this case, there is no evidence for unusual interaction between TPD and PVK that affects the hole transport process.

However, certain synergistic effects have been observed recently in several systems when transport-active polymers are doped with high concentrations of hole-transporting molecules (48, 52). For example, doping with high concentrations of α-phenyl-4-*N,N*-diphenylaminostyrene [89114-90-9] (TPS) 3 (52), tetrakis(3-methylphenyl)-*N,N,N′,N′*-2,5-phenylenediamine [124591-08-8] (PDA) 3 (52), and TPD (3**a**) (48) in PMPS produces samples with hole mobilities of ca 10^{-3} cm^2/Vs (Table 1, entries 19–21), which are higher than in neat undoped PMPS and also higher than these dopants would show if they were dispersed in transport-inactive matrices at the same concentrations. In one instance, *N,N′*-bis(4-methylphenyl)-*N,N′*-bis(4-ethylphenyl)-[1,1′-(3,3′-dimethyl)biphenyl]-4,4′-diamine [115310-63-9] (ETPD) 3 -doped PMPS (Table 1, entry 22), hole mobility approaching 10^{-1} cm^2/Vs at 2.5×10^5 V/cm was observed (48). This is the highest recorded hole mobility for disordered organic systems. From this perceptive, it is very interesting to study the carrier mobility of polymers heavily doped with semiconductor nanoclusters.

3. Charge Generation

Another important property of a photoconductor is the efficiency with which it converts photons into electrons and holes. Most of the photoconductive polymers have low charge-generation efficiencies. This can be a result either of an intrinsically low charge-generation efficiency or of a low absorption coefficient in the interesting spectral region. To enhance the charge-generation efficiency, sensitizers have to be added. Photoexcitation of the sensitizer generates an excited state, which can be either a singlet, triplet, or charge-transfer state. The excited state can relax radiatively or nonradiatively, or undergo electron-transfer reaction. If it accepts an electron from the surrounding polymer, a hole is then generated in the polymer. This initially generated electron–hole pair may recombine to the neutral ground state, or separate under the electric field into free carriers for conduction.

The charge-generation efficiency of a photoconductor can be measured by the standard photoinduced discharge method (33, 67, 68). The sample film is deposited on an electrically grounded aluminum substrate

and corona-charged positively or negatively in the dark. The voltage is detected by an electrostatic voltmeter. Absorption of light generates electrons and holes which migrate to the surface and discharge the voltage if the sample is photoconductive. For light of sufficiently low intensity absorbed within a small fraction of the film thickness (the so-called emission-limited condition), the charge-generation efficiency, φ, can be obtained from the initial discharge rate of the surface potential, $(dV/dt)_{t=0}$ (eq. 6) (33, 67, 68). Here ϵ is the dielectric constant, e the electronic charge, L the film thickness, and I the absorbed photon flux. This technique works best for materials with minimal deep carrier traps.

$$\phi = -\frac{\epsilon}{4\pi eLI}\left(\frac{dV}{dt}\right)_{t=0} \qquad (6)$$

The details of the charge-generation mechanism can be very complicated, requiring a complete understanding of the primary photophysical and photochemical processes. Systematic studies on the charge-generation mechanism are few (69–71). Furthermore, unlike charge transport where the theoretical framework for detailed understanding is available, there is no theoretical model that can adequately address charge recombination and charge separation under electric field quantitatively.

3.1. Onsager Model

The theory developed by Onsager (72) has been the standard model to use for analyzing the electric field dependence of the charge-generation efficiency. The model solves the diffusion equation of the relative motion of an electron–hole pair, bounded by their Coulomb interaction, under an electric field. The origin of the electron–hole pair and the pathway by which it is generated are not considered in this model. The model solves for the probability that the pair separates toward infinity with a given initial separation distance, r_0. An important boundary condition and assumption for this model is that if the pair separation distance reaches zero, the pair recombines immediately. With this assumption, the charge-generation efficiency, $\varphi(r_0, E)$, in the presence of an electric field, E, is given by the following (72, 73):

$$\phi(r_0, E) = \phi_0 \left\{ 1 - (2\xi)^{-1} \sum_{j=0}^{\infty} A_j(\eta) A_j(2\xi) \right\} \qquad (7)$$

where

$$\eta = \frac{e^2}{\epsilon \cdot k \cdot T \cdot r_0} \qquad (8)$$

$$2\xi = \frac{e \cdot E \cdot r_0}{k \cdot T} \qquad (9)$$

$$A_{j+1}(\eta) = A_j(\eta) - \frac{\eta^{j+1} \cdot e^{-\eta}}{(j+1)!} \qquad (10)$$

$$A_0(\eta) = 1 - e^{-\eta} \qquad (11)$$

Here φ_0 is the quantum yield of the initially generated electron–hole pair. The two parameters, r_0 and φ_0, characterize quantitatively the charge generation efficiency of a photoconductor under applied field. For example, a large r_0 value indicates the photoconductor has a large low field charge-generation efficiency while the φ_0 value represents the ultimate charge-generation efficiency achievable at high field.

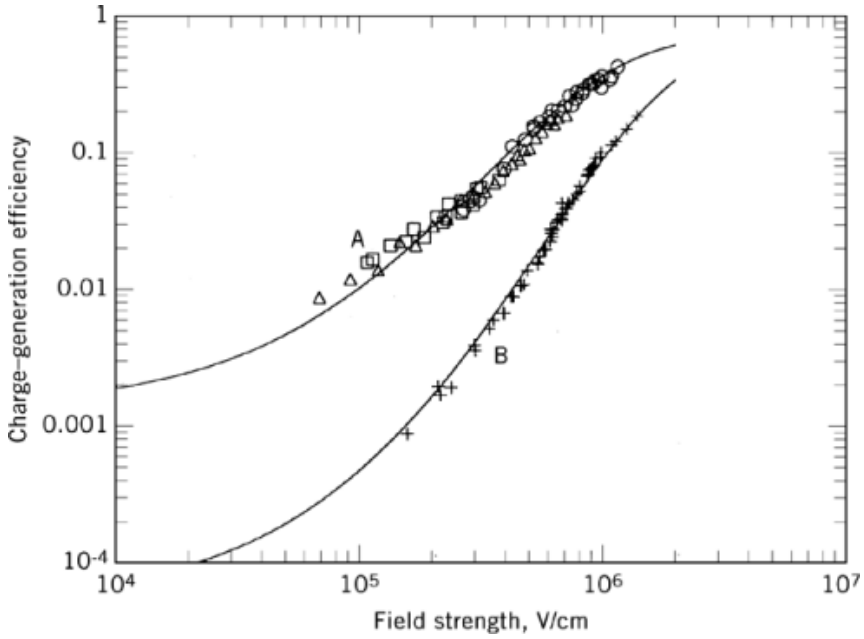

Fig. 7. The field-dependence of the charge-generation efficiency of a 2.0-μm thick (○), a 1.1-μm thick (□), and 1.8-μm thick (△) fullerene/PMPS film obtained with positive charging and 340-nm irradiation (A). The solid lines are calculated from the Onsager model. The best-fit curve is obtained with r_0=2.7 nm and ϕ_0=0.85. Also plotted is the charge-generation efficiency of a fullerene/PVK film (+) obtained with positive charging and 340-nm irradiation (B). The solid lines are calculated from the Onsager model. The best-fit curve is obtained with r_0=1.9 nm and ϕ_0=0.9 (13).

The field dependences of the charge-generation efficiency of many polymeric photoconductors have been analyzed in terms of the Onsager model and found to be in satisfactory agreement. For example, Figure 7 shows the field dependence of the charge-generation efficiencies of fullerene-doped PVK and PMPS. The corresponding fits with the Onsager model yield r_0 = 1.9 nm and ϕ_0 = 0.9 for fullerene-doped PVK; r_0 = 2.7 nm and ϕ_0 = 0.85 for fullerene-doped PMPS (12, 13). This indicates that, in order to explain the field-dependence of the charge-generation efficiency, a fairly large initial electron–hole separation distance of 1.9–2.7 nm must be assumed. For polymeric photoconductors, this finding is quite common. Fitting with the Onsager model always results in large initial electron–hole separation distances with these materials (Table 3). The problem is that such a large initial electron–hole separation distance is improbable in a molecular system. In fact, in many cases it is concluded that charge-transfer state is responsible for the charge generation, which should lead to an initial electron–hole separation distance of only a few tenths of a nanometer. This paradox indicates the inadequacy of the Onsager model and is still an unresolved issue.

3.2. Modified Onsager Models

The boundary condition used in the Onsager model corresponds to the assumption that when the separation distance of an electron–hole pair reaches zero, it recombines with an infinitely fast rate. This assumption is unrealistic in real systems. For an electron–hole pair to recombine to the ground state, several electron volts of energy have to be disposed of, usually by being dumped into the vibrational modes of the system. This can be a slow (eg, nanoseconds) process because of the large amount of energy involved. Next, the creation and

Table 3. Charge-Generation Efficiency of Selected Polymeric Photoconductors[a]

Polymers	r_0, nm	φ_0	Reference
PVK	2.25	0.14 at 345 nm	74
0.1% trichloroacetic acid/PVK	3.0	0.11 at 345 nm	74
6 mol % 2,4,7-trinitro-9-fluorenone/PVK	2.5	0.23 at 550 nm	75
50 mol % 2,4,7-trinitro-9-fluorenone/PVK	3.5	0.23 at 550 nm	75
16% *x*-form metal-free phthalocyanine/PVK		0.4 at 620 nm (1.4×10^6 V/cm)	76
2.7% fullerene/PVK	1.9	0.9 at 340 nm	12
1.6% fullerene/PMPS	2.7	0.85 at 340 nm	13
poly(hydroxyamino ester) (PHA)	3.5	0.02 at 380 nm	51
32% CBr_4/PHA	2.4	0.04 at 380 nm	51
32% CBr_4/PHA + Michler's hydrol blue photolysis products	2.2	1.0 at 630 nm	51
thiapyrylium dye aggregates in TPM/polycarbonate	4.4	0.58 at 680 nm	77
DPBDK/TPA/polycarbonate	3.3	0.53 at 300 nm	78
1 vol % 1.6-nm CdS clusters/PVK	2.6	0.16 at 340 nm	26
BZ perylene		0.1 (8×10^5 V/cm)	84
BZ perylene/TPD bilayer		0.1 (3×10^4 V/cm) 0.6 (8×10^5 V/cm)	79
TPATA		0.06 (2×10^5 V/cm) 0.01 (5×10^4 V/cm)	80
TPATA/amine bilayer		0.8 (8×10^5 V/cm)	80

[a]The initial electron–hole separation distance, r_0, and the quantum yield, φ_0, are derived by fitting with the Onsager model. When the initial quantum yield, φ_0, is not known, the quantum yield at a specified field (in parentheses) is listed. All acronyms are defined in Figures 2 and 3.

recombination rate may depend on the field, separation distance, and energetics. None of these are considered by the Onsager model.

The need for a finite recombination rate has been recognized (81, 82). One suggested model identifies the geminate electron–hole pair with the excited charge-transfer state which typically has a lifetime on the scale of nanoseconds (81). In another model, the escape probability of an electron–hole pair is solved for using a different boundary condition than the original Onsager model (82). The boundary condition corresponds to a finite surface recombination velocity on a partly absorbing sphere of finite radius. Indeed, by assuming a slow recombination rate (taken to be the lifetime of either the charge-transfer state or the singlet state), the field dependence data can be fitted by these modified Onsager models with a small initial electron–hole separation distance (81, 82). However, in these models there is no explanation for the origin of the slow recombination rate and the electric field dependence is not considered. Furthermore, there is no theory for either the creation or the escape rate of the electron–hole pair. Rather, a somewhat arbitrary form for the escape rate is assumed (82).

In principle, Marcus electron–transfer theory can be used to describe the creation and recombination of an electron–hole pair. The Marcus electrontransfer theory can qualitatively explain the origin of the slow recombination rate for a fullerene-doped PVK photoconductor (29). A careful examination of the energetics of the electron-transfer reaction between fullerene and carbazole reveals that the forward electron transfer is exothermic by 0.37 eV, corresponding to the maximum rate region in the Marcus electron-transfer theory (83). However, the backward electron transfer (recombination) is exothermic by 1.52 eV, which falls in the so-called Marcus inverted region (83). In the inverted region, the recombination rate is slower by many orders-of-magnitude. This provides the basic reason for the efficient charge separation in fullerene-doped polymers under applied field. For quantitative comparison with the experimental data, an Onsager-type model incorporating field-dependent Marcus electron-transfer theory needs to be developed.

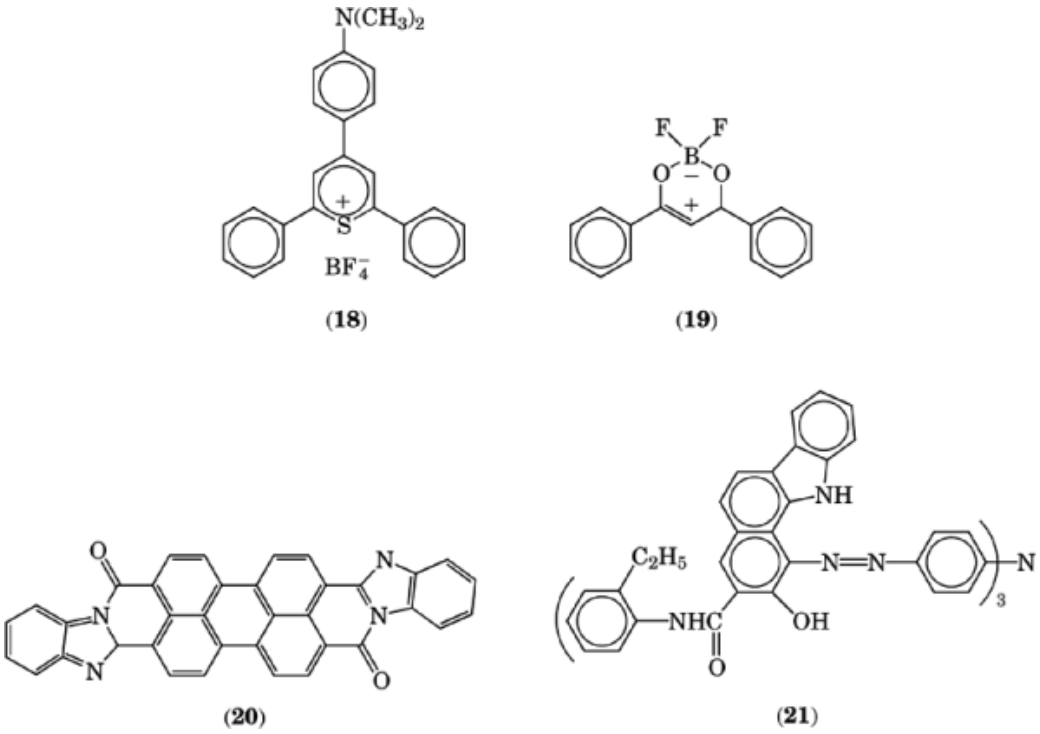

Fig. 8. Molecular structures of selected sensitizers: (**18**) thiapyrylium dye [25966-12-5]; (**19**) difluoroboron-1,3-diphenyl-1,3-propanedionate (DPBDK); (**20**) benzimidazole (BZ) perylene pigment; and (**21**) triphenylamine trisazo pigment (TPATA).

3.3. Experimental Values of Charge-Generation Efficiencies

In this section the charge-generation efficiencies of many polymeric photoconductors are compared (Table 3). When the experimental data has been fitted to the Onsager model, the initial electron–hole separation distance, r_0, and the initial quantum yield, φ_0, are listed. Otherwise, the charge-generation efficiency at selected field is given. Although the Onsager model has its limitations and problems, it nevertheless provides a common platform to compare various photoconductors, since many important photoconductors have been analyzed by this model. Not much significance should be attached to the molecular meaning of r_0.

The intrinsic charge-generation efficiency of polymers is often low and needs to be enhanced by the addition of sensitizers. The sensitizer can be dissolved in the polymer to enhance the bulk charge-generation efficiency of the polymer. Effective sensitizers include 2,4,7-trinitro-9-fluorenone [129-79-3] (TNF), fullerene, thiapyrylium dye, CdS nanoclusters, etc (Table 3). Molecular structures of selected sensitizers are shown in Figure 8.

The charge-generation efficiency of a polymer can also be sensitized externally in a bilayer device. In that case, a sensitizer dye is deposited as a charge-generation layer on top of a polymer film acting as a charge-transport layer. The overall charge-generation efficiency depends not only on the intrinsic charge-generation efficiency of the sensitizer, but also on the electron-transfer efficiency across the interface from the sensitizer to the polymer. It was found that the total charge-generation efficiency of such a bilayer device is often higher than that of the charge-generation layer alone (eg, Table 3) (79, 80). Charge-generation efficiency as high as ca 0.8 at 8×10^5 V/cm has been achieved in a TPATA bilayer device (Table 3). By using TPATA as the charge-generation layer and a series of amines with different redox potential as the charge-transporting layer, it was found that the

charge-generation efficiency depends on the free-energy difference of the interfacial electron-transfer reaction between TPATA and the amines (84). The dependence can be described by the Marcus electron-transfer theory. This result clearly confirms the importance of interfacial electron-transfer in a bilayer device.

4. Applications and Related Technologies

The most important industrial application of photoconductive polymers is electrophotography (qv). This is a billion dollar industry and one of the few electronic areas where polymeric material excels. The principles and practices of electrophotography have been reviewed in detail elsewhere (9, 85) and are not repeated here.

The availability of photoconductive polymers opens up many areas for research, in addition to electrophotography. These are relatively unexplored areas and represent promising future directions.

4.1. Electroluminescence

Photoconductivity is based on the conversion of light to electricity. The reverse phenomenon, electroluminescence, is based on the conversion of electricity to light. Electroluminescence is useful for flat-panel display and II–VI semiconductors such as ZnS are employed for this purpose (85). The current trend is toward the development of polymeric electroluminescent material for their processing flexibility (86–88). Hole-transporting polymers such as poly(*p*-phenylenevinylene) (87) and PMPS (88) have been used in such devices. Semiconductor nanocluster-doped polymers represent another interesting class of materials for the exploration of electroluminescent phenomenon. It has already been demonstrated that properly doped semiconductor nanoclusters such as $Zn_xMn_{1-x}S$ emits light efficiently (89). With the demonstration of photoconductivity (26) these nanocluster-doped polymers can become possible candidates for electroluminescent materials (90).

4.2. Photorefractive Effect

If a material possesses second-order optical nonlinearity and is photoconductive, it may be photorefractive (91). Photorefractivity is a third-order nonlinear optical, $x^{(3)}$, phenomenon. The phenomenon occurs as photogenerated carriers redistribute and create an inhomogeneous space-charge field in the medium. If the material has second-order optical nonlinearity, $x^{(2)}$, this space-charge field can modulate the refractive index of the material through the electrooptical effect. Photorefractive materials provide a medium in which holographic gratings can be reversibly written and are useful as optical interconnects. A good photorefractive material requires large second-order nonlinearity and high charge-generation efficiency.

Recently photorefractivity in photoconductive polymers has been demonstrated (92–94). The second-order nonlinearity is obtained by poling the polymer doped with a nonlinear chromophore. Such a polymer may or may not be a good photoconductor. Usually sensitizers have to be added to enhance the charge-generation efficiency. The sensitizer function of fullerene in a photorefractive polymer has been demonstrated (93).

4.3. Data Storage

An interesting extension of photoconductor technology to optical data storage has been reported (95). The device consists of a solid thin film of the photoconductor, zinc-octakis(β-decoxyethyl)porphyrin, sandwiched between two transparent electrodes. Irradiation by light (550 nm) under an applied electric field generates electron–hole pairs which are separated within the photoconductive layer. When the irradiation is interrupted, these electron–hole pairs become trapped within the film because of the low dark conductivity. This corresponds to the data-writing step. The written information can be read by irradiation of the device with a read beam (at 550 nm) under short circuit conditions. The release of electrons or holes from the traps leads to a photocurrent

spike, which can be taken to represent the memory state, "1," compared with an uncharged state, "0." The basic principle behind this data storage scheme is similar to that of xerography, where the readout method is by toning with carbon particles to form an image (96). The reported method represents a digital way of reading the electrostatic image (95) (see Information storage materials, optical).

This new optical data storage device is reported to be robust and nonvolatile. The response time for the write–read beam is in the subnanosecond range, and no refreshing is required for long-term retention of trapped charges (95). The basic principle may be applied to other, similar photoconductive materials.

BIBLIOGRAPHY

Cited Publications

1. R. B. Seymour, ed., *Conductive Polymers*, Plenum Press, New York, 1981.
2. U.S. Pat. 3,037,861 (June 5, 1962), H. Hoegl, O. Sus, and W. Neugebauer (to Hoechst AG).
3. U.S. Pat. 3,484,237 (Dec. 16, 1969), D. M. Shattuck and U. Vahtra (to IBM).
4. D. Haarer, *Angew. Makromol. Chem.* **183**, 197 (1990).
5. M. Stolka, in J. I. Kroschwitz, ed., *Encyclopedia of Polymer Science and Engineering*, Vol. **11**, Wiley-Interscience, New York, 1987, p. 154.
6. W. D. Gill, in J. Mort and D. M. Pai, eds., *Photoconductivity and Related Phenomena*, Elsevier, Amsterdam, the Netherlands, 1976, p. 303.
7. H. Bässler, *Phys. Stat. Sol.* (*b*) **175**, 15 (1993).
8. J. Mort and G. Pfister, in J. Mort and G. Pfister, eds., *Electronic Properties of Polymers*, John Wiley & Sons, Inc., New York, 1982, p. 215.
9. L. B. Schein, *Electrophotography and Development Physics*, Springer-Verlag, Berlin, 1988.
10. M. Biswas and T. Uryu, *J. Macromol. Sci., Rev. Macromol. Chem. Phys.* **C26**, 248 (1986).
11. W. D. Gill, *J. Appl. Phys.* **43**, 5033 (1972).
12. Y. Wang, *Nature* **356**, 585 (1992).
13. Y. Wang, R. West, and C. H. Yuan, *J. Amer. Chem. Soc.* **115**, 3844 (1993).
14. R. West, in S. Patai and Z. Rappoport, eds., *The Chemistry of Organic Silicon Compounds*, John Wiley & Sons, Inc., New York, 1989, Chapt. 19, 1207–1240.
15. R. D. Miller and J. Michl, *Chem. Rev.* **89**, 1359 (1989).
16. R. G. Kepler, J. M. Zeigler, L. A. Harrah, and S. R. Kurtz, *Phys. Rev. B*, **35**, 2818 (1987).
17. M. Abkowitz, F. E. Knier, H.-J. Yuh, R. J. Weagley, and M. Stolka, *Solid St. Comm.* **62**, 547 (1987).
18. M. Stolka, H.-J. Yuh, K. McGrane, and D. M. Pai, *J. Polym. Sci. Polym. Chem. Ed.* **25**, 823 (1987).
19. M. Fujino, *Chem. Phys. Lett.* **136**, 451 (1987).
20. M. A. Abkowitz, K. M. McGrane, F. E. Knier, and M. Stolka, *Mol. Cryst. Liq. Cryst.* **183**, 157 (1990).
21. S. Morita, S. Kiyomatsu, X. H. Yin, A. A. Zakhidov, T. Noguchi, T. Ohnishi, and K. Yoshino, *J. Appl. Phys.* **74**, 2860 (1993).
22. L. L. Chapoy and co-workers, *Mol. Crysl. Liquid Cryst.* **105**, 353 (1984).
23. L. L. Chapoy and co-workers, *Macromolecules* **16**, 181 (1983).
24. D. Adam and co-workers, *Phys. Rev. Lett.* **70**, 457 (1993).
25. J. Billard, J. C. Dubois, N. H. Tinh, and A. Zahn, *Nouv. J. Chim.* **2**, 535 (1978).
26. Y. Wang and N. Herron, *Chem. Phys. Lett.*, **200**, 71 (1992).
27. U.S. Pat. 5,238,607 (Aug. 24, 1993), (to Du Pont Co.).
28. Y. Wang and N. Herron, *J. Phys. Chem.* **95**, 525 (1991).
29. Y. Wang, in D. C. Neckers, ed., *Advances in Photochemistry*, Vol. **19**, John Wiley & Sons, Inc., New York, 1995.
30. Y. Wang and N. Herron, *Res. Chem. Intermedi.* **15A**, 17 (1991).
31. O. H. Le Blanc, *J. Chem. Phys.* **33**, 626 (1960).

32. K. G. Kepler, *Phys. Rev.*, **199** 1226 (1960).
33. F. K. Dolezalek in J. Mort and D. M. Pai, eds., *Photoconductivity and Related Phenomena*, Elsevier, Amsterdam, the Netherlands, 1976, p. 27.
34. H. Scher and M. Lax, *Phys. Rev. B* **7**, 4491, 4502 (1973).
35. H. Scher and E. W. Montroll, *Phys. Rev. B* **12**, 2455 (1975).
36. H. Bässler, *Philos. Mag. B* **50**, 347 (1984).
37. P. M. Borsenberger, L. Pautmeier, H. Bässler, *J. Chem. Phys.* **94**, 5447 (1991).
38. B. Movaghar, M. Grünewald, B. Ries, H. Bässler, and D. Würtz, *Phys. Rev. B* **33**, 5545 (1986).
39. P. M. Borsenberger, L. Pautmeier, and H. Bässler, *Phys. Rev. B* **46**, 12145 (1992).
40. D. Emin, in P. G. LeComber and J. Mort, eds., *Electronic and Structural Properties of Amorphous Semiconductors*, Academic Press, Inc., New York, 1973, Chapt. 7.
41. L. B. Schein, D. Glatz, and J. C. Scott, *Phys. Rev. Lett.* **65**, 472 (1990).
42. L. B. Schein, *Philos. Mag. B* **65**, 795 (1992).
43. P. M. Borsenberger and L. B. Schein, *J. Phys. Chem.* **98**, 233 (1994).
44. D. M. Pai, *J. Chem. Phys.* **52**, 2285 (1970).
45. Technical data, Du Pont Co., 1995.
46. T. Sasakawa, T. Ikeda, and S. Tazuke, *Macromol.* **22**, 4253 (1989).
47. H. Domes, R. Fischer, D. Haarer, and P. Strohriegl, *Makromol. Chem.* **190**, 165 (1989).
48. M. Stolka and M. A. Abkowitz, *Syn. Met.* **54**, 417 (1993).
49. D. M. Pai, J. F. Yanus, and M. Stolka, *J. Phys. Chem.* **88**, 4714 (1984).
50. J. S. Facci and co-workers, *J. Phys. Chem.* **95**, 7908 (1991).
51. A. Yu. Kryukov, A. A. Pakhratdinov, A. V. Vannikov, A. V. Anikeev, L. I. Kostendo, *Chem. Mater.* **4**, 72 (1992).
52. K. Yokoyama, S. Notsu, and M. Yokoyama, *J. Chem. Soc., Chem. Commun.*, 805 (1990).
53. H. Bässler, *Adv. Mat.* **5**, 662 (1993).
54. H.-J. Yuh and D. M. Pai, *Mol. Cryst. Liquid Cryst.* **183**, 217 (1990).
55. L. B. Schein, A. Rosenberg, and S. L. Rice, *J. Appl. Phys.* **60**, 4287 (1986).
56. P. M. Borsenberger, W. Mey, and A. Chowdry, *J. Appl. Phys.* **49**, 273 (1978).
57. G. Pfister, *Phys. Rev. B* **16**, 3676 (1977).
58. D. M. Pai, J. F. Yanus, M. Stolka, D. Renfer, and W. W. Limburg, *Phil. Mag. B*, **48**, 505 (1983).
59. P. M. Borsenberger, A. Chowdry, D. C. Hoesterey, and W. Mey, *J. Appl. Phys.* **49**, 5555 (1978).
60. T. Ikeda, H. Mochizuki, Y. Hayashi, and M. Sisido, *J. Appl. Phys.* **70**, 3689 (1991).
61. P. M. Borsenberger and J. J. Fitzgerald, *J. Phys. Chem.* **97**, 4815 (1993).
62. P. M. Borsenberger and H. Bässler, *J. Chem. Phys.* **95**, 5327 (1991).
63. P. M. Borsenberger, J. J. Fitzgerald, and E. H. Magin, *J. Phys. Chem.* **97**, 11314 (1993).
64. P. M. Borsenberger, E. H. Magin, and J. J. Fitzgerald, *J. Phys. Chem.* **97**, 8250 (1993).
65. M. Stolka, J. F. Yanus, and D. M. Pai, *J. Phys. Chem.* **88**, 4707 (1984).
66. M. Van der Auweraer, F. C. DeSchryver, P. M. Borsenberger, and J. J. Fitzgerald, *J. Phys. Chem.* **97**, 8808 (1993).
67. P. J. Regensburger, *Photochem. Photobiol.* **8**, 429 (1968).
68. I. Chen and J. Mort, *J. Appl. Phys.* **43**, 1164 (1972).
69. Z. D. Popovic and E. R. Menzel, *J. Chem. Phys.* **71**, 5090 (1979).
70. Z. D. Popovic, *J. Chem. Phys.* **78**, 1552 (1983).
71. M. Yokoyama, S. Shimokihara, A. Matsubara, and H. Mikawa, *J. Chem. Phys.* **76**, 724 (1982).
72. L. Onsager, *Phys. Rev.* **54**, 554 (1938).
73. A. Mozumder, *J. Chem. Phys.* **60**, 4300 (1974).
74. G. Pfister and D. J. Williams, *J. Chem. Phys.* **61**, 2416 (1974).
75. P. J. Melz, *J. Chem. Phys.* **57**, 1694 (1972).
76. C. F. Hackett, *J. Chem. Phys.* **55**, 3178 (1971).
77. P. M. Borsenberger and D. C. Hoesterey, *J. Appl. Phys.* **51**, 4248 (1980).
78. T. E. Goliber, J. H. Perlstein, *J. Chem. Phys.* **80**, 4162 (1984).
79. Z. D. Popovic, A.-M. Hor, and R. O. Loutfy, *Chem. Phys.* **127**, 451 (1988).
80. M. Umeda and M. Hashimoto, *J. Appl. Phys.* **72**, 117 (1992).
81. C. L. Braun, *J. Chem. Phys.* **80**, 4157 (1984).

82. J. Noolandi and K. M. Hong, *J. Chem. Phys.* **70**, 3230 (1979).
83. R. A. Marcus and P. Siders, *J. Phys. Chem.* **86**, 622 (1982).
84. M. Umeda, T. Shimada, T. Aruga, T. Niimi, and M. Sasaki, *J. Phys. Chem.* **97**, 8531 (1993).
85. R. Mach and G. O. Muller, *Phys. Stat. Sol.* **69**, 11 (1982).
86. C. W. Tang and S. A. Vanslyke, *Appl. Phys. Lett.* **51**, 913 (1987).
87. J. H. Burroughes and co-workers, *Nature* **347**, 539 (1990).
88. H. Suzuki, H. Meyer, J. Simmerer, J. Yang, and D. Haarer, *Adv. Mater.* **5**, 743 (1993).
89. Y. Wang, N. Herron, K. Moller, and T. Bein, *Solid State Comm.* **77**, 33 (1991).
90. B. O. Dabbousi and co-workers, *Appl. Phys. Lett.* **66**, 1316 (1995).
91. P. Gunter and J.-P. Huignard, eds., *Photorefractive Materials and Their Applications I and II*, Springer-Verlag, Berlin, 1988 1989.
92. S. Ducharme, J. C. Scott, R. J. Twieg, and W. E. Moerner, *Phys. Rev. Lett.* **66**, 1846 (1991).
93. S. M. Silence, C. A. Walsh, J. C. Scott, and W. E. Moerner, *Appl. Phys. Lett.* **61**, 2967 (1992).
94. J. C. Scott, L. T. Pautmeier, and W. E. Moerner, *Synth. Met.* **54**, 9, 1993.
95. C.-Y. Liu, H.-L. Pan, M. A. Fox, and A. J. Bard, *Science*, **261**, 897 (1993).
96. R. M. Schaffert, *Electrophotography*, Focal Press, London, 1980.

YING WANG
Du Pont Company

Related Articles

Electrically conductive polymers; Information storage materials, optical